Design of complex large-scale photonic integrated circuits (PICs) based on ring-resonator structures

C. Arellano*[a], S. Mingaleev[b], E. Sokolov[b], I. Koltchanov[a], A. Richter[a]
[a]VPIsystems, Carnotstr. 6, 10587 Berlin, Germany;
[b]VPI Development Center, Chapaeva str. 5, 220034 Minsk, Belarus

ABSTRACT

The exponentially growing number of components in complex large-scale Photonic Integrated Circuits (PICs) requires the necessity of photonic design tools with system-level abstraction, which are efficient for designs enclosing hundreds of elements. Ring-resonators and derived structures represent one example for large-scale photonics integration. Their characteristics can be parameterized in the frequency-domain and described by scattering matrix (S-matrix) parameters. The S-matrix method allows time efficient numerical simulations, decreasing the simulation time by several orders of magnitude compared to time-domain approaches yielding a better modeling accuracy as the number of PIC elements increases.

We present the modeling of optical waveguides within a sophisticated design environment using application examples that contain ring-resonators as fundamental structure. In the models, the two orthogonally polarized guided modes are characterized by their specific index and loss parameters. Systematic variation of circuit parameters, such as coupling factor or refractive index, allows a comfortable design, analysis and optimization of many types of complex integrated photonic structures.

Keywords: photonic integrated circuit, ring resonator, ring coupler, photonic waveguide, scattering matrix, design, modeling, photonic integration

1. INTRODUCTION

The number of components in Photonic Integrated Circuits (PICs) emerges exponentially, similar to Moore's law of electronic integrated circuits. The number of elements in most advanced PICs reaches a few hundred already now, especially those in computing [1-2] and networking [3] applications. This leads to the necessity of photonic design tools with system-level abstraction supporting efficient simulations of such structures.

Photonics modeling can be addressed through different approaches depending on the level of the design, from a single device, a transmission link or a large network. In a multi-layer modeling framework [4], the modeling of PICs is placed at a device-level design. Traditional tools based on Finite-Difference Time-Domain (FDTD) method and Beam Propagation Method (BPM) solvers are widely used for modeling small-scale PICs. However, they are not appropriate for modeling large-scale PICs because they are too slow and their layout editors are inconvenient for defining schematics with a large number of elements. Time-domain methods are very competitive for solving light propagation in optical waveguides with arbitrary geometries like multimode interference devices (MMIs) or star couplers but they become highly inefficient for modeling PICs with several sub-components. Moreover, a deep level of detail is not necessary in most of the cases and a description of the device in terms of S-matrices is sufficient. The speed of numerical simulations can be significantly increased by usage of the S-matrix approach, which operates in the frequency-domain. The S-matrix approach has been developed formerly and is widely used in high-frequency electrical engineering to characterize and design microwave circuits. This method can also be applied for the modeling of large-scale photonic crystals [5-6].

Ring-resonators (RRs) and derived structures represent one example for large scale photonics integration, which can be well described by S-matrices. RRs in conjunction with silicon photonics integration technologies are very promising as they offer a growing number of applications such as modulation/demodulation, switches, delay lines and other signal processing tasks [7-8]. After an introduction into the general ideas of the modeling framework in the next section, several ring-resonator applications are presented and discussed in section three of this paper.

*Cristina.Arellano@VPIsystems.com; phone +49-30-398-058-30; fax +49-30-398-058-0; www.VPIphotonics.com

Physics and Simulation of Optoelectronic Devices XIX, edited by Bernd Witzigmann, Fritz Henneberger, Yasuhiko Arakawa, Alexandre Freundlich, Proc. of SPIE Vol. 7933, 79330U · © 2011 SPIE · CCC code: 0277-786X/11/$18 · doi: 10.1117/12.874711

2. MODELING FRAMEWORK

Adhering to the multi-layer methodology for photonics modeling[1] and in order to cover device designs from the system perspective we have developed an original modeling framework that addresses the new and rising demand for PICs simulation tools. Within this framework, basic building blocks of optical waveguide geometries are used as functional elements for transporting signals between different elements in the photonic circuit. The propagation of signals in the photonic waveguides is described by a two-component sampled signal representing the two orthogonally polarized guided modes. TE and TM mode are characterized by their own effective and group mode indices, attenuation and insertion losses, or alternatively, by delay time and optical losses.

We developed models of PIC elements that can work in both, frequency- and time-domain numerical simulations. The frequency-domain models are very time-efficient in simulations of structures with many elements, overcoming one of the main challenges of traditional time-domain Maxwell equation solvers (e.g., FDTD, BPM). Further on, we accomplished accurate time-domain simulations of PICs through an advanced method for modeling finite-impulse response (FIR) filters. So, the modeling of waveguide-based elements can be combined with other systems-level models of semiconductor cavities using either domain. Active devices such as semiconductor lasers, amplifiers, and absorbers for instance are modeled favorably in the time-domain by means of the Transmission-Line Laser-Model [9-10]. In this model, the semiconductor cavity is numerically discretized into several subsections, where for each one of them the bidirectional laser rate equations are solved. Both types of elements, active and frequency-domain represented (mainly passive), can interoperate in a same simulation schematic.

Ring resonator structures concerting this paper are passive elements, which can be represented by several building blocks emulating the characteristics of geometrical substructures. We identified two key building blocks, namely: ring resonator and ring coupler, and different connector blocks, namely y-branch, y-combiner, x-coupler and straight waveguide elements (Figure 1). They can all be described and modeled in the same way by introducing referenced scattering-matrices. The S-matrix contains the complex-valued, frequency-dependent components describing transfer functions for input/output ports of the photonic element. The photonic circuit can be solved by multiplication or convolution of those matrices in the frequency- or time-domain, respectively (Figure 2). This representation of a PIC device can be applied either in the frequency- or time-domain, depending on the periodicity/aperiodicity of processed signals and the presence/absence of active devices in the modeled circuit. In the S-matrix approach, all passive PIC devices are considered as mere multi-port and/or multi-mode optical filters, and therefore, can be combined with systems-level models of other components and subsystems such as fibers, optical amplifiers, electrical components, receivers including performance estimation modules, for instance, and simulated altogether in the same schematic. S-matrix can be loaded from data files defined by measurements, for instance, or can be calculated by using approximate analytical models that are specific for each type of PIC device. For MMI devices, S-parameters are calculated analytically with the self-imaging matrix model [11]. The analytical model for star coupler elements is based on field transformation through a finite Fourier transform. S-parameters are calculated analytically in paraxial approximation using the Fourier optics model. S-parameters for straight waveguides are calculated on the basis of waveguide length, attenuation, mode coupling coefficient, effective and group mode indices and dispersion. The analytical models of ring resonator and ring coupler are explained in detail in the next section.

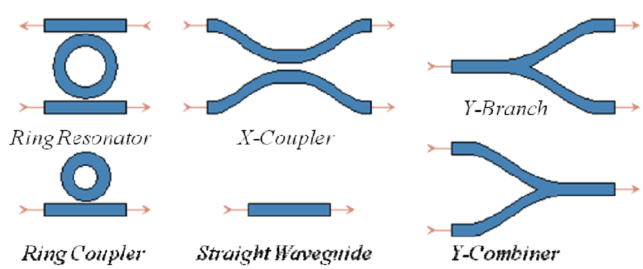

Figure 1. Basic building blocks for modeling ring-resonator structures.

[1] provided, for instance, in the professional design suite *VPIcomponentMaker* / *VPItransmissionMaker*.

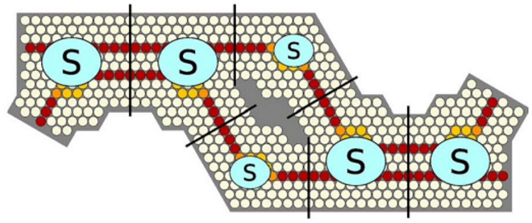

Figure 2. Representation of a photonic circuit by discretization of S-matrices [6].

In our modeling framework for passive PICs, each device is considered as a black box, characterized by several ports, enumerated from 1 to N (Figure 3). Each port represents a device connection point through which optical signals come in/out to the device. In most cases, ports can be associated with photonic wire waveguides.

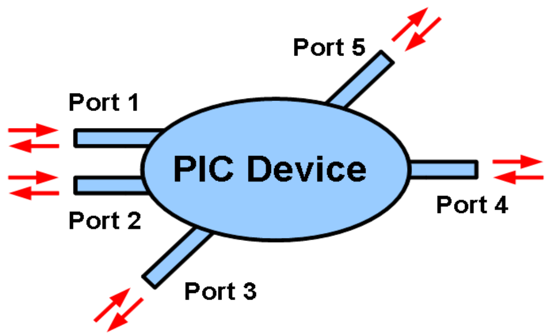

Figure 3. Representation of a 5-port PIC device. Transfer functions between each port are represented by S-parameters, forming the S-matrix of the PIC device.

Ports can be intrinsically multimode, however, here we consider that each port supports exactly two polarization modes, a TE-like mode in the E_x component and a TM-like mode in its E_y component of the signal field representation. Ports of physical PIC devices are intrinsically bidirectional so back reflections and polarization coupling might occur. The resulting S-matrix of the modeled passive PIC device is a matrix of complex frequency-dependent functions (transfer functions) that multiplied in frequency-domain (or convolved in the time-domain) with the input signals produces the output signals. Denoting the spectra of input and output signals at port n as $\vec{E}_n^{(\mathrm{in})}(f)$ and $\vec{E}_n^{(\mathrm{out})}(f)$, we can write the filtering in frequency-domain as:

$$\begin{pmatrix} \vec{E}_1^{out} \\ \vec{E}_2^{out} \\ \cdots \\ \vec{E}_N^{out} \end{pmatrix} = \hat{S}(f) \begin{pmatrix} \vec{E}_1^{in} \\ \vec{E}_2^{in} \\ \cdots \\ \vec{E}_N^{\mathrm{in}} \end{pmatrix} \tag{1}$$

where the S-matrix $\hat{S}(f)$ consists of NxN Jones matrices $\hat{T}_{nm}(f)$ connecting input port m with the output port n. In its turn, each Jones matrix is formed by four complex-valued frequency-dependent transfer functions: $T_{nm}^{TE,TE}(f)$, $T_{nm}^{TE,TM}(f)$, $T_{nm}^{TM,TE}(f)$, and $T_{nm}^{TM,TM}(f)$. Once the frequency dependencies of all the transfer functions constituting the S-matrix of the modeled passive PIC device are known, Eq. (1) is applied for obtaining output signals from the input signals in the frequency-domain.

2.1 Analytical model for Ring Resonator

The Ring Resonator structure consists of an optical waveguide bended into a circle and placed close to a straight waveguide, so coupling between these two elements occurs. The resultant magnitude of the transfer function is unit for all frequencies while its group delay has maxima at resonance frequencies (Figure 4). This element acts as an all-pass phase shifter. The resonance frequencies are determined by the length of the waveguide forming the ring. Inside the ring, the spectrum of the circulating signal has maxima at resonance frequencies. The S-matrix of the RR can be either loaded from file or calculated analytically. If an analytical description is applied, the S-matrices are determined on the basis of the following physical parameters [12]. The RR can be designed either for getting the desired resonance properties (specified by Free Spectral Range - FSR, design polarization, resonance frequency, and Q-factor) or on the basis of structure parameters (specified by parameters coupling waveguide-ring, ring length and ring phase shift). Attenuation in the ring and bus are also considered.

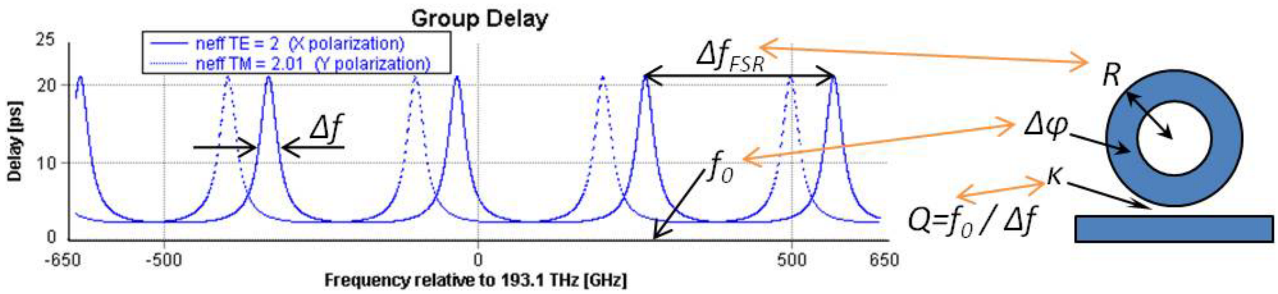

Figure 4. Group delay of the transfer function of a single-ring resonator for two polarizations (left) and RR structure (right).

The considered analytical model does not account for back reflections. Hence, transfer functions for $n=m$ in Eq. (1) are zero. Therefore, the only non-trivial transfer functions will be those that connect input waves at left port with output waves at right port (and vice versa) for the same polarization:

$$\begin{pmatrix} E_{2,TE}^{\text{out}}(f) \\ E_{2,TM}^{\text{out}}(f) \end{pmatrix} = \begin{pmatrix} T_{2,1}^{TE,TE}(f) & 0 \\ 0 & T_{2,1}^{TM,TM}(f) \end{pmatrix} \begin{pmatrix} E_{1,TE}^{\text{in}}(f) \\ E_{1,TM}^{\text{in}}(f) \end{pmatrix} \tag{2}$$

The two non-zero transfer function coefficients are calculated as outlined in [12] and are equal to:

$$T_{2,1}^{TE,TE}(f) = \frac{t_{TE} - \exp(-j\theta_{TE}(f))}{1 - t_{TE} \cdot \exp(-j\theta_{TE}(f))} \exp\{-j\tilde{\beta}_{TE,bus}(f) L_{bus}\} \tag{3}$$

$$T_{2,1}^{TM,TM}(f) = \frac{t_{TM} - \exp(-j\theta_{TM}(f))}{1 - t_{TM} \cdot \exp(-j\theta_{TM}(f))} \exp\{-j\tilde{\beta}_{TM,bus}(f) L_{bus}\} \tag{4}$$

Here, the following notations have been introduced:

$t_{TE} = \sqrt{1 - K_{TE}}$; $t_{TM} = \sqrt{1 - K_{TM}}$; $\theta_{TE}(f) = \tilde{\beta}_{TE,ring}(f) \cdot L_{ring} - \varphi_{TE,ring}$; $\theta_{TM}(f) = \tilde{\beta}_{TM,ring}(f) \cdot L_{ring} - \varphi_{TM,ring}$

with $\tilde{\beta}_{TE,ring}$and $\tilde{\beta}_{TM,ring}$being generalized complex-valued propagation constants of TE- and TM-like guided modes in the ring waveguide. Accordingly, $\tilde{\beta}_{TE,bus}$ and $\tilde{\beta}_{TM,bus}$are generalized complex-valued propagation constants of TE- and TM-like guided modes in the bus waveguide. Here, propagation constants include also mode attenuation:

$$\tilde{\beta}_{TE,ring}(f) = \frac{2\pi f}{c} n_{eff,TE}(f) - \frac{j}{2} \alpha_{TE,ring} \tag{5}$$

with similar expressions (using different attenuation constants) for the three other propagation constants.

The attenuation inside the ring waveguide can be specified either explicitly or by specifying the desired loss per one roundtrip along the ring waveguide. With the length of the ring waveguide L_{ring}, the attenuation constants are calculated for the latter case as $\alpha_{TE,ring}^{dB} = TurnLoss_{TE}/L_{ring}$ and $\alpha_{TM,ring}^{dB} = TurnLoss_{TM}/L_{ring}$. The frequency dependence of the effective indices $n_{eff,TE}(f)$ and $n_{eff,TM}(f)$of TE- and TM-like modes is assumed to be equal in both bus and ring waveguides, and is found from the parameters effective index, group index and reference frequency and dispersion.

The other parameters are length of the ring waveguide, L_{ring}; coefficients K_{TE} and K_{TM} , describing power coupling between the bus and ring waveguides; and additional phase shifts, $\varphi_{TE,ring}$and $\varphi_{TM,ring}$, added to accumulated complex phases of both modes in the ring waveguide can be either specified explicitly or calculated automatically for the desired resonance properties. The latter case is realized by specifying the desired resonance properties free spectral range, resonance frequency and the resonance quality factor which may be specified for each polarization individually. With this, the corresponding structure parameters can be calculated from simple expressions.

2.2 Analytical model for Ring Coupler

The Ring Coupler (RC) structure is formed by two bus waveguides coupled to a RR. A single RC acts as an efficient add-drop filter (Figure 5). The analytical model of the RC is very similar to the ring resonator, with the difference that two coupling coefficients are considered for the ring and upper and lower waveguides.

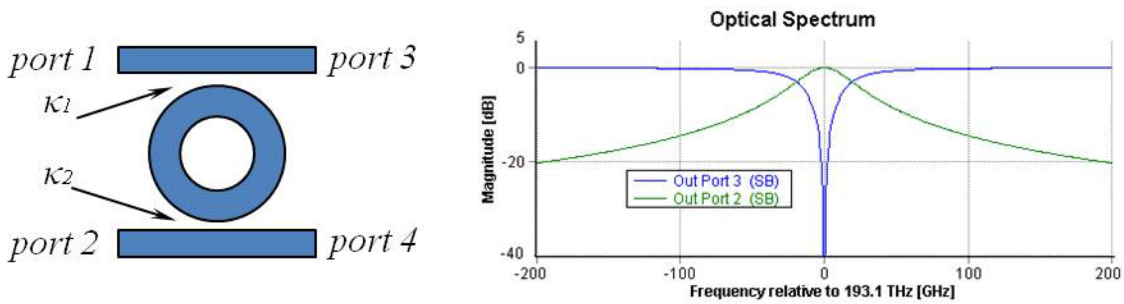

Figure 5. Schematic of the ring coupler structure and magnitude of the transfer function at ports 2 and 3 when an input signal is applied at port 1.

In a simplified model of the RC, neither back reflections nor TE/TM mode coupling is considered, as in the RR model. Therefore, for *n*=*m* transfer functions are zero and there is no coupling between signals in ports 1 and 3 and in ports 2 and 3. Consequently, the only non-trivial transfer functions are those that connect input waves at ports 2 and 3 with output waves at ports 1 and 4 (and vice versa), for one polarization. Here, we consider as an example the expressions for TE-polarization (they are functionally the same for the TM-polarization), so output fields are described as:

$$\begin{pmatrix} E_{1,TE}^{\text{out}}(f) \\ E_{4,TE}^{\text{out}}(f) \end{pmatrix} = \begin{pmatrix} T_{1,2}^{TE,TE}(f) & T_{1,3}^{TE,TE}(f) \\ T_{4,2}^{TE,TE}(f) & T_{4,3}^{TE,TE}(f) \end{pmatrix} \begin{pmatrix} E_{2,TE}^{\text{in}}(f) \\ E_{3,TE}^{\text{in}}(f) \end{pmatrix} \tag{6}$$

The transfer function coefficients are calculated similar as for the RR case [12]:

$$T_{1,2}^{TE,TE}(f) = T_{4,3}^{TE,TE}(f) = \frac{\kappa_{TE}^{up}\kappa_{TE}^{low}\exp(j\theta_{TE}(f)/2)}{t_{TE}^{up}t_{TE}^{low} - \exp(j\theta_{TE}(f))}\exp\{-j\tilde{\beta}_{TE,bus}(f)L_{bus}\} \tag{7}$$

$$T_{4,2}^{TE,TE}(f) = \frac{t_{TE}^{up} - t_{TE}^{low}\exp(j\theta_{TE}(f))}{t_{TE}^{up}t_{TE}^{low} - \exp(j\theta_{TE}(f))}\exp\{-j\tilde{\beta}_{TE,bus}(f)L_{bus}\} \tag{8}$$

$$T_{1,3}^{TE,TE}(f) = \frac{t_{TE}^{low} - t_{TE}^{up}\exp(j\theta_{TE}(f))}{t_{TE}^{up}t_{TE}^{low} - \exp(j\theta_{TE}(f))}\exp\{-j\tilde{\beta}_{TE,bus}(f)L_{bus}\} \tag{9}$$

where coupling (k), transfer (t) and propagation (β) coefficients follow analogue expressions as for the RR, described in the previous section. The RC can be also designed either for getting the desired resonance properties or on the basis of structure parameters.

3. DESIGN EXAMPLES

In this section we demonstrate the applicability of the developed modules using examples of a tunable delay, tunable filter, ring-loaded Mach-Zehnder (MZ) interferometer, channel add-drop multiplexer and MZ modulator with cascaded rings. The investigated examples are based on real devices that have been recently reported.

3.1 Tunable delay

A tunable delay device can be implemented by two cascaded ring-resonators (Figure 6). Such structure finds applications in microwave photonics as it is sensitive to power changes in the RF frequency range. The tunability is achieved by means of the thermo-optic effect in silicon material [13]. This property involves changes in the refractive index by deploying thermal heating. The heating of the rings is controlled electrically, varying the power at electrodes placed next to the coupling positions, so the thermo-optic effect is mostly used for tuning devices with a moderate number of elements.

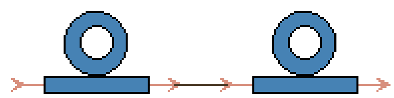

Figure 6. Schematic of the cascaded two-ring resonator

The two rings are designed with identical geometries, so the resultant transfer function has a maximum delay at the resonance frequency. When modifying the electrical power at the rings, the effective length of the device changes and thus, its resonance frequency. By keeping one of the rings with a constant power and tuning the other one, the resonant offset increases and the resulting resonances and notch might become flat for a certain value of detuning, as shown in Figure 7. This would be the optimum case as the phase shifting would be achieved without variation in the RF range [14].

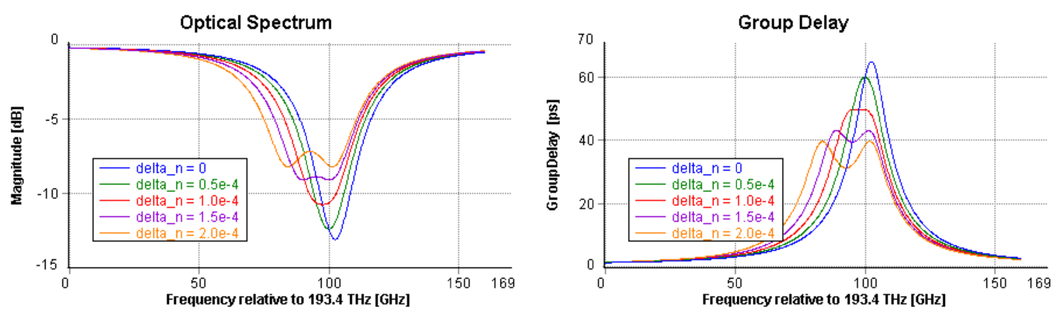

Figure 7. Magnitude and group delay of the two-ring resonator transfer function. Ring lengths and waveguides are 110 um, 55 um, respectively; attenuation inside the ring is 1500 dB/m; and coupling factor waveguide-ring 0.1.

3.2 Ring-Loaded Mach-Zehnder

A device named ring-loaded Mach-Zehnder interferometer (MZI) comprises a MZI with a delay-ring in one of its arms. This arrangement might perform as an interleaver filter [15-16] with symmetrical transfer functions on Bar and Cross ports when the length difference of the branches is correctly designed, specifically, the length unbalance is one half of the length of the ring. In our design, represented in Figure 8 (left), the ring is 500 um and the bottom waveguide is 250 um long. The magnitude of the transfer function at the Bar and Cross outputs is represented in Figure 8 (right). The resultant FSR is 600 GHz, which can be also calculated as $FSR = c/n_{eff}\Delta L$; being c the velocity of light, n_{eff} the effective index (set to 2) and ΔL the path difference.

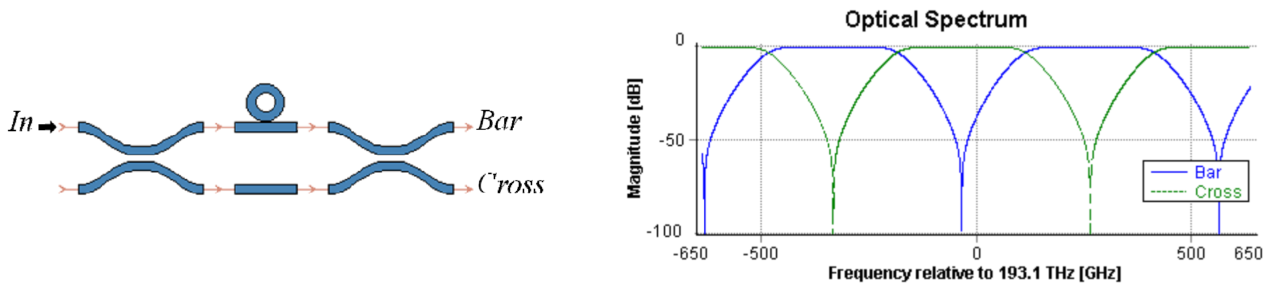

Figure 8. Schematic of the Ring-Loaded MZ (left). Magnitude of the transfer function at Bar and Cross outputs (right).

The transfer function shown in Figure 8 represents the optimum case, achieved for ideal couplers (coupling factor 0.5 at input and output ports) and for coupling ring-waveguide (K_r) of 0.9. However, characteristics of a real physical device might suffer from effects such as different refractive indices at the ring and the waveguides, non-ideal couplers, and imperfect matching of waveguide lengths. All these aspects are easy to investigate by numerical simulations which might also help to optimize the device. Figure 9 (left) shows the magnitude of the transfer function at the Bar output for different values of the ring-waveguide coupling. Ripple occur in the passbands for values diverting significantly from the optimum one. In Figure 9 (right), the parameter K_r has been kept at its optimum and the coupling coefficient of one of the couplers has been varied, representing a frequency-dependent splitting ratio. The extinction ratio deteriorates considerably for small variations of the coupling.

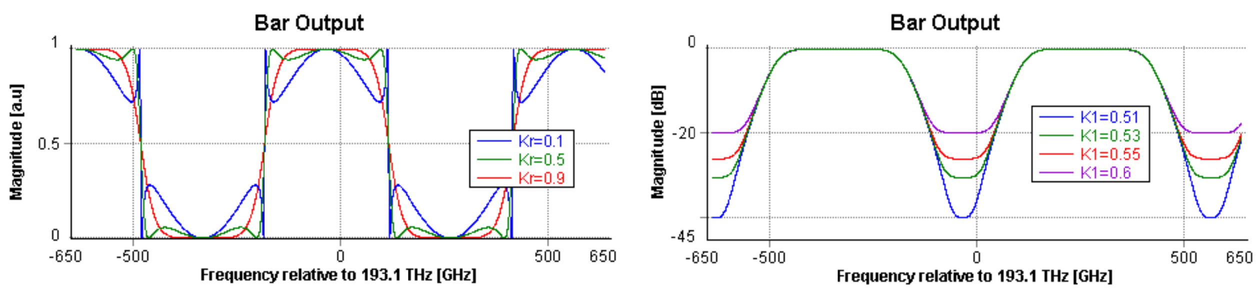

Figure 9. Magnitude of the transfer function at Bar output for different values of the coupling coefficient at the ring (left) and coupler (right).

3.3 Tunable Filter

By increasing the complexity one step and introducing a second ring in the MZI structure, Figure 10 (left), a bandwidth tunable optical filter can be implemented [17]. Electrical electrodes at the rings are used to act on its length and phase shift by deploying thermal heating and changing the resonance frequency via the thermo-optic effect. By keeping the properties of one of the rings constant and varying the resonance frequency of the other one, the bandwidth tunability is achieved, as represented in Figure 10 (right). Up to 50GHz bandwidth can be achieved with less than 3 dB ripple in the transmission response.

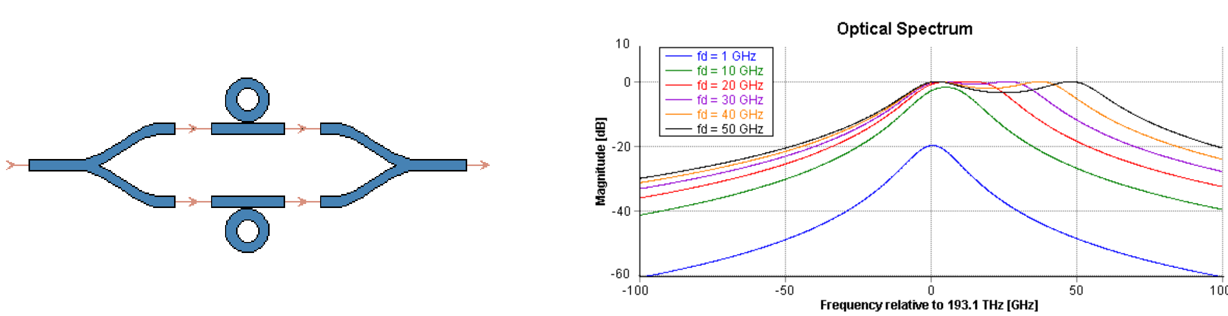

Figure 10. Diagram of the tunable filter device (left) and magnitude of its transfer function for different values of frequency offset applied at one of the rings (right).

3.4 Four-Channel Add-drop Multiplexer

Next we show an example which uses ring couplers (RC) as elementary elements. The device consists of four cascaded RCs, representing a 4-channel add-drop multiplexer [18] (Figure 11). Each RC is tuned to the resonance frequency of the desired channel. Again, tunability might be achieved by thermal heating with electrodes attached to the rings.

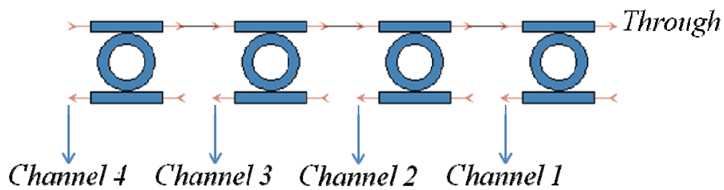

Figure 11. Diagram of the 4-channel Add-drop Multiplexer.

Figure 12 (left) shows the magnitude of the transfer function at the through and drop output ports. Figure 12 (right) demonstrate the drop of the four channels. It can be observed that channel 4 is not affected by adjacent sub-channels, however, channels 1 to 3 present interferences at the center frequency, coming from resonances of the adjacent channel. By slightly tuning the resonance frequencies and Q-factors this effect might be investigated and optimized.

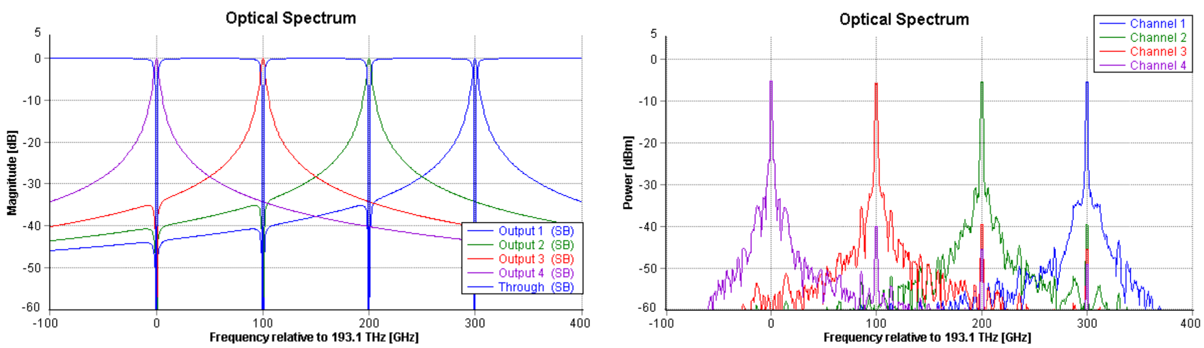

Figure 12. Magnitude of the transfer function at channel and through outputs (left). Signal at output ports for a WDM input signal (right).

3.5 Mach-Zehnder with cascaded Ring Resonators

The last application example that is discussed here is a modulator consisting of a Mach-Zehnder interferometer loaded with a 10-cascaded ring resonator (Figure 13). This type of device presents better modulation efficiency when compared with a conventional MZM having a similar footprint size [19]. Here we want to point out that the design of a device with a large number of elements (here: a total of 22) does not imply a huge degree of complexity in editing or analyzing the design. As illustration, a single parameter control may be defined that allows automatic variation of the group velocity inside the device. Figure 14 shows corresponding transfer functions at output ports over a large spectral range.

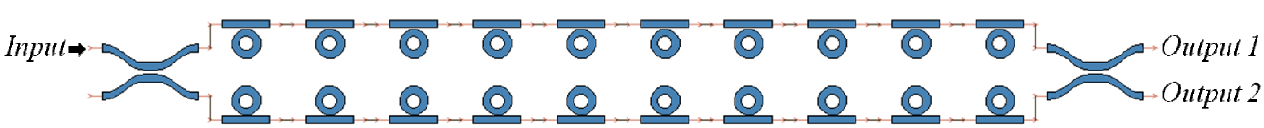

Figure 13. Schematic of the 10-cascaded ring Mach-Zehnder device.

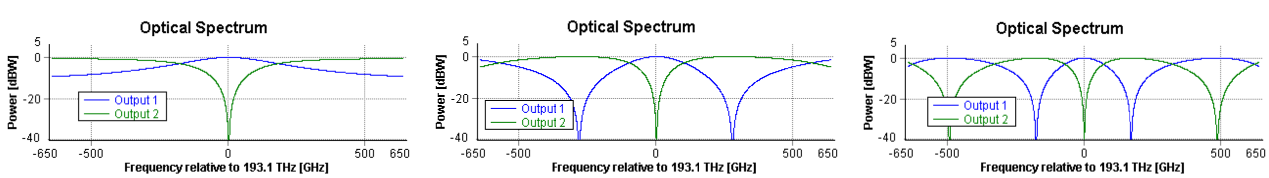

Figure 14. Magnitude of the transfer function at output ports for different values of group velocity inside the structure.

Effective and group indices might differ for different polarizations; in fact, they are very different in SOI devices. Exemplary, Figure 15 shows transfer functions for TE and TM polarizations of the same device considering different values of group and effective indices for the two polarizations. It illustrates a different constellation of resonance frequencies that might impact severely polarization multiplexed systems, for instance, and should be taken into account in the design. The degree of degradation of the system might be further investigated by systematic numerical simulations.

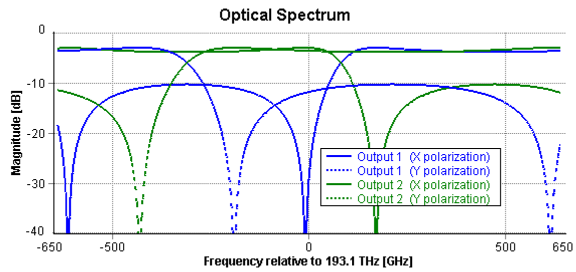

Figure 15. Magnitude of the transfer function at output ports for the two polarizations TE and TM. Group and effective indices for TE and TM are, respectively, n_{grTE} =4, n_{grTM} =3, n_{effTE} =2.6, n_{effTM} =2.2.

4. SUMMARY

We presented a modeling framework for the design of photonic integrated circuits (PICs) and discussed application examples that contain ring-resonators as fundamental structure. Among many other modeling features, the framework includes a family of basic PIC elements and a methodology for numerical simulations based on the S-matrix method. The discussed level of modeling PICs allows a seamless integration with other systems-level simulation techniques. Analytical models for S-matrix calculations of ring resonator and ring coupler have been exposed and demonstrated in several integrated device applications. The presented examples enclose passive elements only allowing numerical simulations to be carried out entirely in the frequency-domain. The S-matrix approach deployed in the frequency-domain allows the simulation of highly integrated designs consisting of a large number of elements with competitive time and accuracy.

ACKNOWLEDGEMENTS

The research leading to these results has received funding from the European Union Seventh Framework Program FP7/2007-2013 under grant agreement n° 257980 (MIRTHE).

REFERENCES

[1] www.research.ibm.com/photonics
[2] http://techresearch.intel.com/ResearchAreaDetails.aspx?Id=26
[3] Albores-Mejia, A., Gomez-Agis, F., Dorren, H.J.S., Leijtens, X.J.M., Smit, M.K., Robbins, D.J. and Williams, K.A., "320Gb/s Data Routing in a Monolithic Multistage Semiconductor Optical Amplifier Switching Circuit," Proc. ECOC, We.7.E.1 (2010).
[4] Richter, A., Louchet, H., Arellano, C., Farina, J., Koltchanov, I., "Multi-layer photonics modeling framework for the design, analysis, and optimization of devices, links, and networks," SPIE Photonics West 2011, OPTO, paper 7959-20 (2011).
[5] Mingaleev, S. F. and Busch, K., "Scattering matrix approach to large-scale photonic crystal circuits," Opt. Lett. 28, 619–621 (2003).
[6] Hermann, D., Schillinger, M., Mingaleev, S.F. and Busch, K., "Wannier-function based scattering-matrix formalism for photonic crystal circuitry," J. Opt. Soc. Am. B, 25(2), 202-209 (2008).
[7] Reed, G. T., Mashanovich, G., Gardes, F. Y. and Thomson, D. J., "Silicon optical modulators," Nature Photonics 4, 518-526 (2010).

[8] Leuthold, J. , Koos, C. and Freude , W., "Nonlinear silicon photonics", Nature Photonics 4, 535-544 (2010).
[9] Lowery, A.J., "A new dynamic semiconductor laser model based on the transmission line modeling method," IEE Proc. J. Optoelectron., 134 (5) (1987).
[10] Arellano, C., Mingaleev, S.F., Novitsky, A., Koltchanov, I., Richter, A., "Design of Complex Semiconductor Integrated Structures," ACP, paper WD4 (2009).
[11] Heaton, J.M. and Jenkins, R.M., "General Matrix Theory of Self-Imaging in Multimode Interference (MMI) couplers," IEEE Phot. Tech. Lett., 11(2) (1999).
[12] Yariv, A. "Universal relations for coupling of optical power between microresonators and dielectric waveguides," Elec. Lett. 36 (4), 321-322 (2000).
[13] Soref, R.A. and Bennet, B.R., "Electrooptical Effects in Silicon," IEEE Journ. Q. Elect., 23(1) (1997).
[14] Pu, M., Xue, W., Liu, L., Ou, H., Yvind, K. and Hvam, J. M., "360° Tunable Microwave Phase Shifter Based on Silicon-on-Insulator Dual-Microring Resonator," Proc. ECIO, paper WeD3 (2010).
[15] Roeloffzen, C.G.H., Ridder, R.M., Sengo, G., Wörhoff K. and Driessen, A., "Passband flattened interleaver using a Mach-Zehnder interferometer with ring resonator fabricated in SiON waveguide technology," Proc. Symposium IEEE/LEOS Benelux Chapter, 32-35 (2002).
[16] Song, J., Fang, Q., Tao, S.H., Yu, M.B., Lo, G.Q. and Kwong, D.L.,"Passive ring-assisted Mach-Zehnder interleaver on silicon-on-insulator," Opt. Express, 16(12), 8359-8365 (2008).
[17] Ding, Y., Zhang, X., Huang, D., Pu, M., Liu, L., Xu, J., Peucheret, C. and Ou, H., "Bandwidth tunable filter based on silicon microring-MZI structure", Proc. ECIO, paper ThP20 (2010).
[18] Geng, M., Jia, L., Zhang, L., Yang, L., Chen, P., Wang, T. and Liu, Y., "Four-channel reconfigurable optical add-drop multiplexer based on photonic wire waveguide", Opt. Express, 17 (7), 5502-5516 (2009).
[19] Akiyama, S., Kurahashi, T., Baba, T., Hatori, N., Usuki, T. and Yamamoto, T., "Slow-Light Silicon Mach-Zehnder Modulator Based on Cascaded Ring Resonators", Proc. CLEO/QELS, paper CTuHH5 (2010).